

Dynamics and lifetime of geometric excitations in moiré systems

Yuzhu Wang,¹ Joe Huxford,² Dung Xuan Nguyen,^{3,4} Guangyue Ji,⁵ Yong Baek Kim,² and Bo Yang¹

¹*School of Physical and Mathematical Sciences, Nanyang Technological University, 639798 Singapore*

²*Department of Physics, University of Toronto, Toronto, Ontario M5S 1A7, Canada*

³*Center for Theoretical Physics of Complex Systems,*

Institute for Basic Science (IBS), 34126 Daejeon, Korea

⁴*Basic Science Program, Korea University of Science and Technology (UST), 34113 Daejeon, Korea*

⁵*Department of Physics, Temple University, Philadelphia, Pennsylvania, 19122, USA*

(Dated: February 6, 2025)

We show that spin-2 geometric excitations, known as graviton modes, generally exhibit vanishing lifetimes in lattice Chern bands, including in moiré systems. In contrast to the Landau levels, we first numerically demonstrate that the prominent graviton peaks in spectral functions diminish rapidly with increasing system sizes. We explore how the choice of interaction affects the strength of these peaks, with short-ranged interactions pushing the graviton mode far into the continuum of excitations, where it can be significantly scattered due to the increased density of states. We also analytically investigate the short lifetime of the graviton mode. In lattice systems, continuous rotational symmetry is broken, leading to highly anisotropic gapped excitations that mix different angular momentum or “spins”. This is despite the surprising emergence of a “guiding center” continuous rotational symmetry in the ground state, which is shared by the graviton mode. Consequently, the graviton mode in Chern bands can be strongly scattered by the anisotropic gapped excitations. However, the emergent rotational symmetry implies that gravitons can be robust in principle, and we propose experimental tuning strategies to lower the graviton mode energy below the continuum. We argue this is a necessary condition enabling the observation of graviton modes and geometric excitations in realistic moiré systems.

I. INTRODUCTION

Neutral excitations in two-dimensional (2D) topological phases have been one of the focuses of recent experimental and theoretical studies [1–12]. They encode both universal topological properties and important dynamical details of the exotic phases of matter [13–18]. Notable examples of such 2D topological phases include strongly correlated topological bands, which can manifest in both conventional lattices and moiré systems, with or without an external magnetic field [19–28]. In partially filled topological bands with narrow bandwidths, electron-electron interactions dominate the physics, resulting in ground states with non-trivial topological orders and various emergent excitations. These excitations, arising from the collective motion of electrons, have been extensively studied in the context of fractional quantum Hall (FQH) systems. Among these, Girvin-Macdonald-Platzman (GMP) modes constitute a distinctive branch of low-lying neutral excitations that define the neutral gap of the FQH fluid [29–31]. At long wavelengths, these modes exhibit a quadrupolar structure, transitioning into a dipolar character as the momentum increases [32, 33].

The long-wavelength behavior of GMP modes in FQH is especially intriguing because of the inherent non-commutative quantum geometry of Landau levels (LLs) [34]. In this context, the GMP mode represents an area-preserving diffeomorphism within the non-commutative guiding center space [15, 35–38]. These excitations originate from quantum fluctuations of the *many-body* metric emerging from the strong interactions and are therefore referred to as “graviton modes (GMs)” in the FQH liter-

ature [15, 39]. The LLs are thus a fascinating platform for studying a non-relativistic quantum gravity in a two-dimensional space [40, 41]. The existence of emergent GMs and their chiralities has been experimentally verified in Abelian fractional quantum Hall states using polarized Raman scattering [11], directly confirming their universal properties [39, 42–44]. Moreover, certain FQH phases with more intricate Hilbert space structures can give rise to multiple GMs, each corresponding to fluctuations of different conformal Hilbert space metrics [43–46]. Signatures of multi-graviton modes have been predicted at specific filling fractions, such as $\nu = 2/7$ and $\nu = 2/9$, providing deeper insights into the geometric degrees of freedom in FQH phases.

Recent advancements in experiments on the quantum anomalous Hall effect (QAHE) and fractional Chern insulators (FCIs) have shown that FQH-like phenomena can emerge in lattice systems with topologically nontrivial flat bands, even in the absence of an external magnetic field [47–52]. This significant breakthrough has been corroborated by experimental observations of robust fractional Hall conductance [47, 48], local thermodynamic gap [51], and the imaging of edge states [52]. In addition, there is significant numerical evidence confirming that essential features from FQH phases are present, including topological degeneracy, entanglement spectra, and quasiparticle statistics [23, 24, 53–57]. The LLs are the simplest topological bands, with zero bandwidth and a uniform quantum geometric tensor, while in 2D quantum materials hosting FCI phases, the band curvature is nonvanishing and the quantum geometry is nonuniform. It is thus natural to ask whether GMs can also emerge in

these more intricate topological bands. Moreover, these systems provide an opportunity to explore physics beyond the conventional LL paradigm. The richer quantum geometry and reduced symmetry of the FCIs suggest that the behavior of GMs in these systems could differ significantly, potentially revealing new insights into the interplay of topology, geometry, and dynamics in fractionalized topological phases.

In this paper, we explore the graviton-like excitations in the moiré systems such as twisted bilayer graphene (TBG), where FCI phases have been observed [22]. We extract the essential physics using a simplified ideal flat band (IFB) model, revealing that GMs are significantly weaker compared to the FQH case [58–63]. Our numerical results indicate a rapid decay of the GM lifetime as the density of states (DOS) increases, suggesting that the observed behavior may be strongly influenced by finite-size effects. In particular, with Coulomb interactions, a peak in the spectral function emerges in small systems just above the continuum boundary. However, in the thermodynamic limit where the DOS diverges in the continuum, this resonance peak may disappear. Additionally, we show analytically that the suppression of GM lifetimes is due to the strong scattering between different angular momentum sectors, despite the surprising robustness of guiding center rotational invariance of the ground states. Both our analytic and numerical results should be applicable for generic Chern bands, and we suggest a potential approach to stabilize GMs in experimental settings in such systems.

This paper is organized as follows: In Section II, we introduce the IFBs and geometric excitations in FQH/FCI phases. In Section III, we focus on the chiral limit of TBG (cTBG), which forms IFBs that closely resemble LLs, and show the *significantly weaker* spectral peaks of the GMs at filling $\nu = 1/3$ in IFBs than in the LLs. In Section IV, we examine the DOS to quantitatively confirm such differences in geometric excitations in LLs and IFBs. In Section V, we propose a perturbative model Hamiltonian to explain the sensitivity of the GMs to perturbations. We further investigate these phenomena in more realistic models of MoTe₂ in Section VI, and propose an interaction that can significantly enhance the GM lifetime, guiding potential experimental probes of GMs in FCI phases.

II. MOIRÉ IDEAL FLAT BANDS AND GEOMETRIC EXCITATIONS

The absence of a strong magnetic field in FCIs necessitates the fine-tuning of band properties, including bandwidth, topological invariants, and quantum geometry, to support the emergence of FCI phases [25, 58, 64–66]. While toy models based on Checkerboard [23, 54, 55], Ruby [67], and Kagome [53] lattices have been proposed to achieve such conditions, an appropriate experimental platform to realize FCIs remained elusive until the dis-

covery of moiré systems, such as TBG [22] and twisted transition metal dichalcogenides (tTMDs) [47–50].

We aim to examine the effect of quantum geometry and lattice symmetry on the GMs generally, but are particularly interested in the case of TBG. In the Bistritzer-MacDonald model, the interlayer coupling is described by two parameters, w_{AA} and w_{AB} , which give the interlayer tunneling in the AA and AB regions respectively [68–70]. When w_{AA} is neglected, TBG enters the so-called *chiral limit*, where the band at charge-neutrality becomes perfectly flat at the magic angles, with Chern number $\mathcal{C} = 1$. While this chiral limit is not entirely realistic (the ratio w_{AA}/w_{AB} is approximately 0.7–0.8 [71, 72]), it serves as a good starting point for examining the effect of nonuniform quantum geometry on the GMs. In addition, it has been suggested that the ground state wavefunctions for the realistic case are adiabatically connected to the chiral limit [70], in which case we expect our general conclusions to hold in experimental settings. We will further explain that the general results obtained from the chiral limit hold beyond this idealized case in Section V.

In the chiral limit, the TBG band also becomes an IFB. This type of band is the simplest non-trivial generalization of the LLs, where the fluctuation of the Berry curvature $\Omega_{\mathbf{k}}$ and the quantum metric $g_{\mathbf{k}}^{ab}$ are “in sync” [59–61], with the latter becoming positive definite. This relationship is captured by [58–61]:

$$g_{\mathbf{k}}^{ab} = \frac{1}{2} \omega^{ab} \Omega_{\mathbf{k}}, \quad (1)$$

where ω^{ab} is a positive symmetric matrix with $|\omega^{ab}| = 1$. In experimental systems without a magnetic field, particularly twisted MoTe₂ (tMoTe₂), the Chern bands hosting FCI phases are nearly ideal but do not exactly satisfy Eq. 1 [70, 73].

The LLs represent a special case of IFBs, where the quantum geometry is independent of \mathbf{k} and thus uniform, and the only difference between a generic IFB and a LL is the form factor. Under these conditions, an exact mapping can be established between the wavefunctions ψ of LLs to the wavefunctions $\tilde{\psi}$ of IFBs, provided the modulated quantum geometry is properly accounted for. This mapping is given by [61]:

$$\tilde{\psi}_{\mathbf{k}}(\mathbf{r}) = \mathcal{N}_{\mathbf{k}} \cdot \mathcal{B}(\mathbf{r}) \cdot \psi_{\mathbf{k}}(\mathbf{r}), \quad (2)$$

where $\mathcal{N}_{\mathbf{k}}$ is a normalization factor and $\mathcal{B}(\mathbf{r})$ is quasi-periodic over the unit cell. These functions encode the quantum geometry fluctuations of the band, with the Berry curvature given by [61]

$$\Omega_{\mathbf{k}} = -1 + \Delta_{\mathbf{k}} \ln \mathcal{N}_{\mathbf{k}}, \quad (3)$$

where $\Delta_{\mathbf{k}}$ is the Laplace operator in momentum space.

$\mathcal{B}(\mathbf{r})$ introduces a lattice structure (defined by primitive reciprocal lattice vectors \mathbf{b}) into the wavefunctions so that it breaks the continuous translational symmetry in the many-body ground states. This can be codified by

writing

$$|\mathcal{B}(\mathbf{r})|^2 = \sum_{\mathbf{b} \in \text{RLV}} w_{\mathbf{b}} e^{i\mathbf{b} \cdot \mathbf{r}}, \quad (4)$$

where RLV is the set of all reciprocal lattice vectors. The Fourier coefficients $w_{\mathbf{b}}$ then modify the form factor of the band, giving [61]

$$\begin{aligned} \mathcal{F}(\mathbf{k}_1, \mathbf{k}_2) &:= \langle \mathbf{k}_1 | e^{i(\mathbf{k}_1 - \mathbf{k}_2) \cdot \mathbf{r}} | \mathbf{k}_2 \rangle \\ &= \mathcal{N}_{\mathbf{k}_1} \mathcal{N}_{\mathbf{k}_2} \sum_{\mathbf{b}} w_{\mathbf{b}} f_{-\mathbf{b}}^{\mathbf{k}_1, \mathbf{k}_2}, \end{aligned} \quad (5)$$

where $f_{-\mathbf{b}}^{\mathbf{k}_1, \mathbf{k}_2}$ is the form factor in the LLL:

$$f_{-\mathbf{b}}^{\mathbf{k}_1, \mathbf{k}_2} = \langle \mathbf{k}_1 | e^{i(\mathbf{k}_1 - \mathbf{k}_2 + \mathbf{b}) \cdot \mathbf{r}} | \mathbf{k}_2 \rangle_{\text{LLL}}.$$

As a result, the interaction Hamiltonian in the second quantized form, when projected to the IFB, is given by

$$\begin{aligned} H_{\text{int}} &= \sum_{\mathbf{k}_1, \mathbf{k}_2 \in \text{BZ}} \sum_{\mathbf{q}} V(\mathbf{q}) \mathcal{F}(\mathbf{k}_1, \mathbf{k}_1 + \mathbf{q}) \mathcal{F}(\mathbf{k}_2, \mathbf{k}_2 - \mathbf{q}) \\ &= \sum_{\mathbf{q}} V(\mathbf{q}) \sum_{\mathbf{k}_1, \mathbf{k}_2 \in \text{BZ}} \sum_{\mathbf{b}_1, \mathbf{b}_2} c_{\mathbf{k}_1}^\dagger c_{\mathbf{k}_2}^\dagger c_{\mathbf{k}_2 - \mathbf{q}} c_{\mathbf{k}_1 + \mathbf{q}} \\ &\quad w_{\mathbf{b}_1} w_{\mathbf{b}_2} f_{-\mathbf{b}_1}^{\mathbf{k}_1, \mathbf{k}_1 + \mathbf{q}} f_{-\mathbf{b}_2}^{\mathbf{k}_2, \mathbf{k}_2 - \mathbf{q}} c_{\mathbf{k}_1}^\dagger c_{\mathbf{k}_2}^\dagger c_{\mathbf{k}_2 - \mathbf{q}} c_{\mathbf{k}_1 + \mathbf{q}}. \end{aligned} \quad (6)$$

This formalism allows the interaction physics in IFB to be described in terms of the lowest Landau level (LLL), except with a modified interaction that allows Umklapp processes. For IFBs, it has been established that the leading Umklapp processes dominate, so the relevant quantum geometry of the system can be characterized by only two parameters [61]. w_0 describes the uniform part of the geometry, while w_1 gives the Fourier component for each of the smallest non-zero reciprocal lattice vectors, which we take to have the same weight. This means that setting $w_1 = 0$ results in uniform quantum geometry, reducing the system to the LLL on torus geometry. On the other hand, for the IFB in cTBG, continuum model calculations indicate that the ratio is $w_1/w_0 \sim 0.24$ [61]. By modifying the parameter w_1 , we can tune the quantum geometry of the system, offering a minimal model for comparing the GMs between LLs and moiré systems.

To calculate the response of GMs, the ground-state metric can be deformed in two ways: The first approach employs a one-body operator to construct microscopic trial wavefunctions within the single-mode approximation (SMA) [29]:

$$|\psi_{\mathbf{q}}\rangle = \lim_{q \rightarrow 0} \frac{1}{\sqrt{S_{\mathbf{q}}}} \delta \hat{\rho}_{\mathbf{q}} |\psi_0\rangle, \quad (7)$$

because for translationally invariant ground states, the leading contribution of $\delta \hat{\rho}_{\mathbf{q} \rightarrow 0}$ acts as the generator of area-preserving deformations [15, 35–37, 74]. Here $S_{\mathbf{q}}$

is the projected static structure factor and $\delta \hat{\rho}_{\mathbf{q}} = \hat{\rho}_{\mathbf{q}} - \langle \psi_0 | \hat{\rho}_{\mathbf{q}} | \psi_0 \rangle$ is the regularized density operator, both projected to a single Chern band. In particular, for LLs $\hat{\rho}_{\mathbf{q}}$ represents the guiding center density operator. On compact manifolds such as spheres or tori, however, the momentum \mathbf{q} becomes a discrete quantum number, and accessing the long-wavelength limit requires taking the thermodynamic limit.

The second approach to perturbing the metric involves a two-body chiral graviton operator [44, 75–77], which corresponds to the spin- ± 2 components of the kinetic part of the LLL stress tensor [44, 78]:

$$\hat{O}_{\pm} = \sum_{\mathbf{q}} (q_x \pm iq_y)^2 V(\mathbf{q}) \hat{\rho}_{\mathbf{q}} \hat{\rho}_{-\mathbf{q}}, \quad (8)$$

where $(q_x \pm iq_y)^2$ represents a chiral d-wave symmetry (the magnetic length $\ell_B \equiv 1$) and the LLL form factor $e^{-|\mathbf{q}|^2/2}$ has been absorbed into $V(\mathbf{q})$. The chiral graviton operator \hat{O}_{\pm} and the SMA operator $\delta \hat{\rho}_{\mathbf{q} \rightarrow 0}$ in gapped FQH states are related to each other through the LLL Ward identities [79]. These two approaches differ in their universality and sensitivity to interaction details: The SMA operator is universal, as it captures neutral excitations arising from density modulations of the ground state. In contrast, chiral graviton operators are influenced by specific interaction details and characterize global metric deformations. Both the SMA operator and the chiral graviton operators are experimentally accessible through Raman scattering [11, 30, 39, 45, 78, 80], their measured spectral functions are related to each other by sum rules [39, 42, 45]. Chiral graviton operators can also be directly realized by tilting the magnetic field [38, 76, 81, 82] or applying acoustic waves [75]. Both operators can be extended to IFBs by appropriately adjusting the form factors to account for the discrete translational symmetry of the Hamiltonian and the nonuniform quantum geometry.

To predict the coupling strength of chiral GM in circularly polarized Raman scattering experiments, one can calculate the spectral function [11, 78]:

$$I(E) = \sum_n \left| \langle n | \hat{G} | 0 \rangle \right|^2 \delta(E - E_n + E_0), \quad (9)$$

where E_0 is the ground state energy and \hat{G} can be either $\delta \hat{\rho}_{\mathbf{q} \rightarrow 0}$ or \hat{O}_{σ} . In IFBs (including LLs), the energy and lifetime of GMs can be extracted from $I(E)$: the position of the resonance peak provides an estimate of the GM energy, while the width of the resonance peak reflects the lifetime of the particle or state. A broader peak indicates a shorter lifetime, consistent with the intrinsic limitations imposed by the uncertainty principle.

III. GRAVITON LIFETIME IN MOIRÉ IFBS

Building on the formalism presented in the previous section, we numerically compute the GM spectral func-

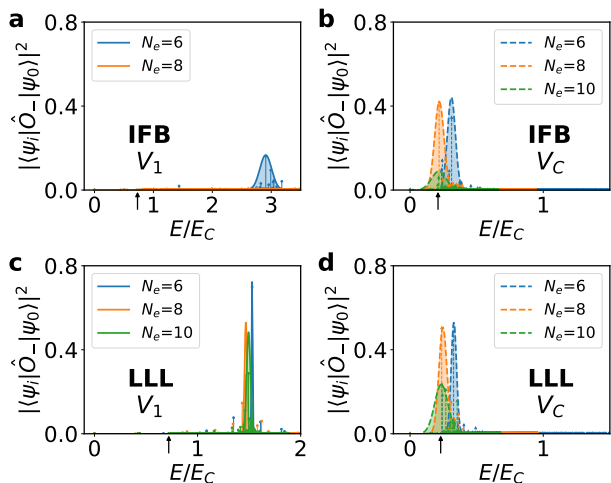


FIG. 1. Spectral functions of the chiral graviton operator at the filling $\nu = 1/3$ in moiré IFB and the LLL. All the spectral peaks shown in this paper have been normalized. The system sizes are distinguished by different colors. Arrows denote the boundary positions of the excitation continuum. The energy scale is determined by the Coulomb energy $E_C = e^2/(4\pi\epsilon l)$, where the characteristic length scale $l = \ell_B$ for LLL and $l = \sqrt{\sqrt{3}/4\pi a_M}$ for IFB. Here a_M is the moiré lattice constant. (a, b) In the IFB of cTBG, a sharp peak persists under V_C even as the system size increases. However, with the V_1 pseudopotential, the energy doubles compared to the LLL and dives deeper into the continuum, while the peaks become significantly suppressed as the system size slightly grows. (c, d) In the LLL, clear and sharp peaks are observed across all system sizes for both the Coulomb interaction V_C (dashed stems) and the V_1 pseudopotential (solid stems). The model Hamiltonian exhibits a particularly pronounced peak, consistent with previous studies on the LLL in torus geometry. These indicate a much shorter GM lifetime in moiré IFBs compared to LLLs.

tions for various system parameters and interactions. These results enable us to predict the signal strength in polarized Raman scattering experiments for GM detection in moiré systems [78]. By comparing the LLL and the moiré IFBs, we find that the GM lifetime of the latter becomes significantly shorter under model Hamiltonians. For simplicity we use the parameters of the IFB from cTBG and only keep the leading Umklapp process [61]. However, all our numerical results and the analytic proof later apply to generic IFB with an arbitrary quasiperiodic $\mathcal{B}(r)$ in Eq. 4.

Focusing on the $1/3$ filling, where the ground states are Laughlin states with three-fold degeneracy, we analyze the GM spectral functions using two types of interactions: the Coulomb interaction $V_C(\mathbf{q}) \sim 1/|\mathbf{q}|$ and the Haldane pseudopotential $V_1(\mathbf{q}) \sim \mathcal{L}_1(|\mathbf{q}|^2)$ (where $\mathcal{L}_m(x)$ denotes the Laguerre polynomials). It is important to note that for both the LLL and moiré IFB, the model $V_1(\mathbf{q})$ Hamiltonian gives the optimal topological phase with the largest incompressibility gap and exact ground

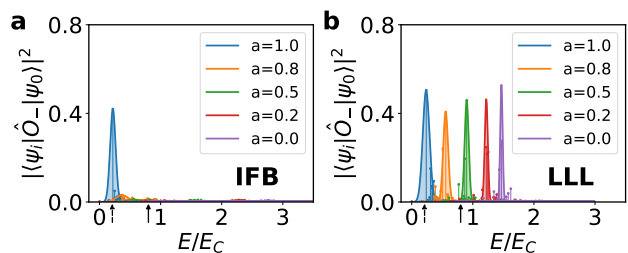


FIG. 2. Spectral function of the toy Hamiltonian V_a at $\nu = 1/3$ with $N_e = 8$. (a) In moiré IFBs, reducing the range of the interaction (reducing a) significantly suppresses the peak magnitude. (b) However, in the LLL, increasing the range of the interaction does not result in significant changes to the highest peak magnitude.

state degeneracy even for finite systems [13, 61, 83–85]. The computed spectral functions for the LLL and moiré IFBs are presented in Fig. 1, where numerical results confirm that GM peaks with positive chirality are suppressed in all scenarios (so only the negative chirality results are shown), resulting in strong selection rules for Raman channels.

For the Coulomb interaction, the peaks in moiré IFB (dashed stems in Fig. 1b) are only slightly lower than those in the LLL (dashed stems in Fig. 1a) for the same system sizes. However, for V_1 in IFBs, increasing the system size strongly suppresses the peaks, as shown in Fig. 1b. To further investigate this behavior, we employ the following toy model:

$$V_a(\mathbf{q}) = a \cdot V_C(\mathbf{q}) + (1 - a) \cdot V_1(\mathbf{q}), \quad a \in [0, 1], \quad (10)$$

to compare the effects in both systems. The results, presented in Fig. 2, reveal a striking contrast between different systems. In the LLL, the GMs under both the V_1 and Coulomb interactions are highly robust, despite significant differences in their respective eigenstates. In moiré IFBs, however, the behavior is different. While the V_1 and Coulomb ground states remain in the same topological phase and show a substantial overlap (~ 0.97 for $N_e = 10$), the corresponding GMs (overlap ~ 0.85 for $N_e = 10$) display distinctly different dynamics. These numerical results on finite systems seem to suggest that, unlike in the LLL, the GM dynamics in moiré IFBs are highly sensitive to *specific interactions*, even if such interactions are adiabatically connected leading to the *same topological phase*. Surprisingly, for a model Hamiltonian where the optimal topological phase is realized with an exact ground state, the GM appears to be the weakest.

IV. FINITE SIZE EFFECT IN MOIRÉ SYSTEMS

A more detailed analysis is needed to understand this unexpected observation that the GM lifetime can be qualitatively different for different interactions within the

same topological phase. From the numerical perspective, the lifetime of the GM, or any trial state, is determined both by the nature of the interaction and the number of eigenstates into which it can scatter (which is system size dependent). In the LLL, the optimal interaction for the GMs aligns with the optimal interaction for the topological phase (e.g., V_1 for the Laughlin phase at $1/3$): the GMs with V_1 exhibit higher peaks, despite a significantly higher DOS near the graviton energy, as compared to the realistic Coulomb interaction [43, 77, 86].

In the case of the IFB, this behavior is reversed: GMs with V_1 have vanishing lifetimes compared to those under Coulomb interactions, as illustrated in the previous section. However, one should note that the DOS near the graviton energy is *much higher* for the V_1 interaction compared to that for the Coulomb interaction. This raises the question: is the weak GM from the V_1 interaction simply a result of the large DOS in the numerical computation? If that is the case, the large GM peak with Coulomb interaction is due to the small DOS for the finite system sizes we consider; in the thermodynamic limit when the DOS diverges even for the Coulomb interaction, the GM lifetime may also vanish in contrast to the case in LLs. This implies that the GMs may be very difficult to observe in experiments.

We now carry out the DOS analysis based on three key observations: first, the energy of the Coulomb and the V_1 GM differs at the same system size; second, a higher GM energy or a larger system results in an increased DOS at a given system size or energy respectively (as shown in Fig. 3); third, higher DOS correlates with reduced spectral peak intensity (as shown in Fig. 1). These trends are consistent across both LLs and moiré IFBs. Moreover, all numerical results are from finite systems, where the spectral functions can be particularly sensitive to the DOS. Thus, controlling the DOS is essential to address the incoherent spectral peaks observed for different interactions in moiré IFBs.

To investigate the difference between the LLL and IFB, we control the DOS and the interaction type. The orange lines in Fig. 3 show the DOS for $N_e = 8$, with panels (a) and (b) presenting the DOS for the Coulomb interaction (V_C) and V_1 , respectively. These results indicate that the DOS at the Coulomb GM energy is comparable for the LLL and IFBs of the same system size, whereas the DOS for V_1 exhibits significant variation. By increasing the system size to $N_e = 10$, we observe that the DOS in the LLL at the GM energy becomes nearly identical to the DOS in moiré IFBs with $N_e = 8$, as illustrated in Fig. 3b.

With both the interaction and the DOS effectively matched, one would expect the GM peaks in the spectral function to show similar profiles for the two systems, if the GMs in the LLL and moiré IFBs share the same physical nature. However, the spectral function for $N_e = 10$ with the V_1 pseudopotential in the LLL still exhibits a remarkably sharp peak, but the corresponding $N_e = 8$ IFB peak is almost completely destroyed, as shown in

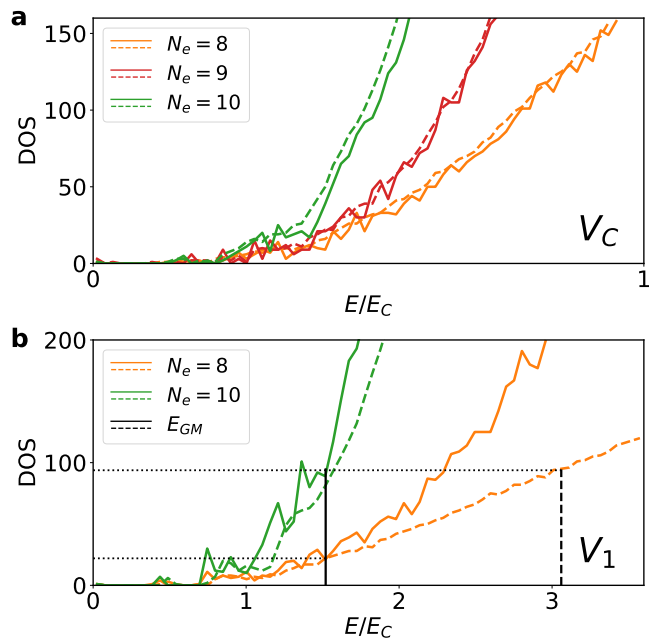


FIG. 3. **DOS plots with different settings.** The DOS is defined as the number of states within each interval of $(E_{\max} - E_0)/\Delta$, where E_{\max} is the upper bound of E -axis, E_0 is the ground state energy and we choose $\Delta = 70$. The lowest 3000 eigenstates within the ground state sector are considered. Colors denote different system sizes. Solid lines represent the DOS values in the LLL, while dashed lines are for the IFB. (a) and (b) depict the DOS for the Coulomb interaction and the V_1 pseudopotential, respectively. The horizontal line indicates the approximate magnitude of the DOS at the GM energy E_{GM} . Notably, in panel b, the DOS at the GM energy for the LLL with $N_e = 10$ (where a sharp GM peak can be observed as shown in Fig. 1c) is nearly identical to that of the moiré IFB with $N_e = 8$.

Fig. 1. This counterexample strongly suggests that the rapid decay of the GM peak in moiré IFBs with V_1 at larger system sizes is closely tied to the specific characteristics of the system itself.

Next, we control the DOS and the system to understand the effect of the interaction. On the LLL, it is well established that for the GM of the Laughlin phase at $1/3$, V_1 consistently produces the most robust and well defined GM when all other conditions are the same [38, 43, 86]. However, the numerical results in the previous section suggest that this may not hold in IFBs, where the significant DOS differences are ignored. To address this, we resolve the DOS discrepancy by comparing moiré IFBs with V_1 and V_C at different system sizes for getting close DOS values: As shown in Table I, the DOS for V_C with $N_e = 10$ is approximately $2/3$ that of V_1 with $N_e = 6$. Despite this, the maximal spectral peak intensity (I_{σ}^{\max}) for V_C is lower, and the peak becomes more spread out (as indicated by the total overlap in a comparable interval around the GM energy) than for V_1 . This result

\hat{H}	N_e	E_g	DOS at E_g	Total Overlap	I_σ^{max}	DOS at I_σ^{max}
\hat{V}_1	6	3.1913	168	0.66163	0.16	153
\hat{V}_C	6	0.3211	19	0.60647	0.42	20
	8	0.2914	51	0.30813	0.35	18
	10	0.2967	115	0.58172	0.12	31

TABLE I. **Comparison of the spectral peaks in moiré IFBs with different interactions and system sizes.** E_g denotes the GM energy, and the DOS is given by the number of states within the interval $[E_g - \Delta/2, E_g + \Delta/2]$, where Δ for $N_e = 6$ with V_1 is set as 0.6 (around $E_g/5$), while dE of Coulomb systems is rescaled by the ratio of GM energy, thus around 0.06. For $N_e = 10$ with Coulomb, even if the DOS is still lower than $N_e = 6$ with V_1 , the peak is lower and broader than the latter. Thus in IFBs, for the same DOS, V_1 still gives a more well defined GM than Coulomb.

demonstrates that even in IFBs, V_1 produces a more robust GM than V_C once the DOS is controlled. It further suggests that the high GM peaks observed for V_C in previous numerical results for moiré bands arise from the significantly lower DOS in smaller systems, and these peaks will diminish as system sizes increase [87].

Combining the analysis above, we conclude that in moiré IFBs, the GM differs qualitatively—and potentially fundamentally—from those in the LLL, regardless of the interaction, even though the system remains in the same topological phase. The physics of the GM in moiré IFBs is still best captured by the V_1 interaction in large systems. The corresponding model GM, originating from the V_1 ground state, exhibits a notably shorter lifetime compared to its counterpart in the LLL. Additionally, in numerical studies, the GM lifetime in moiré IFBs is primarily determined by the DOS unlike in the LLL. In this case, sharp peaks can be observed for both V_1 and Coulomb interactions, provided the DOS is small, suggesting that these observed peaks in moiré systems are very likely *finite-size effects*. Thus in experiments, unless the GM energy lies below the continuum, where the DOS remains small even in the thermodynamic limit, the GM will be challenging to observe.

V. THE MOIRÉ SYSTEM AS PERTURBED LLS

The weakness of the GMs in IFBs, or the moiré systems in general, can be understood analytically using a minimal model based on cTBG. In this section, we show that there is an emergent continuous rotational symmetry projected into the moiré Chern bands for the ground state. This projected rotational symmetry is analogous to the guiding center rotational symmetry in the Landau levels, which is the only rotational symmetry relevant to the dynamics within a single band [15, 83]. Even for a general Chern band, this rotational symmetry can be very robust if the incompressibility gap is present. The GMs excited from the ground state thus have a well-defined spin. However, the broken continuous rotational symme-

try for the *gapped excitations* causes the spin-2 GMs to scatter across all angular momentum sectors. The significantly increased scattering channels suppress the GM peaks in the spectral function, making it much more challenging to observe GMs in IFBs, or lattice Chern bands in general.

To demonstrate this, we first consider a simple first-quantization picture for the interaction in the IFB. Given that the dynamical behavior of GMs is entirely encoded within the intraband properties [15, 38, 43, 44, 77], we ignore the single-particle normalization factor, $\mathcal{N}_{\mathbf{k}}$, in Eq. 2, to simplify our analytical analysis [88]. When we do so, the electrons in the IFB, interacting via $V(\mathbf{r}_1 - \mathbf{r}_2)$, can be mapped on to electrons in a LLL, interacting via the effective interaction [61]:

$$\tilde{V}(\mathbf{r}_1, \mathbf{r}_2) = |\mathcal{B}(\mathbf{r}_1)|^2 |\mathcal{B}(\mathbf{r}_2)|^2 V(\mathbf{r}_1 - \mathbf{r}_2). \quad (11)$$

Because $|\mathcal{B}(\mathbf{r})|^2$ is periodic over the unit cell, we see that this effective interaction breaks the continuous translational symmetry in the LLL down to the discrete translational symmetry of the IFB. For simplicity, we retain only the terms linear in w_1 in Eq. 6 to construct a minimal model to capture the essential physics. In this case, the symmetry breaking part of the interaction can then be written as

$$\delta V(\mathbf{r}_1, \mathbf{r}_2) = 2w_1 w_0 \sum_{\mathbf{b}} e^{i\mathbf{b} \cdot \mathbf{R}} \cos\left(\frac{1}{2}\mathbf{b} \cdot \mathbf{r}\right) V(\mathbf{r}) \quad (12)$$

where $\mathbf{r} = \mathbf{r}_1 - \mathbf{r}_2$ is the relative coordinate and $\mathbf{R} = \frac{\mathbf{r}_1 + \mathbf{r}_2}{2}$ is the centre-of-mass coordinate, and the summation is over the smallest reciprocal lattice vectors (sRLV). One can prove analytically that, with the shortest range interaction for fermions, $V(\mathbf{r}) = \nabla'' \delta(\mathbf{r})$, the isotropic Laughlin state at $\nu = 1/3$ is the exact zero energy state for the effective LLL model [89]. This is despite the explicit breaking of the continuous rotational symmetry of the Hamiltonian, which is evident in the anisotropic dependence of $\delta V(\mathbf{r}_1, \mathbf{r}_2)$ on the center-of-mass coordinate \mathbf{R} . We therefore see that the excited states will generally be affected by scattering that changes the total angular momentum of a pair of electrons, while the ground state remains isotropic.

While this argument shows the emergent rotational symmetry of the ground state, despite the effective interaction breaking the symmetry, it is quite particular to the IFB. By considering the interaction in momentum basis, we can obtain expressions that may be more easily generalizable to other Chern bands. To do this, we again use the expression for the full Hamiltonian given in Eq.6 and ignore the normalization factors. This time, however, we use the relation [61]

$$f_{-\mathbf{b}_i}^{t, t+q} = \eta(\mathbf{b}_i) e^{-\frac{1}{4}|\mathbf{b}_i|^2} e^{-it \times \mathbf{b}_i} e^{\frac{1}{2}\mathbf{b}_i^* q} f_{\mathbf{0}}^{t, t+q}, \quad (13)$$

with the complex variables $q = q_x + iq_y$, $\mathbf{b}_i = b_{i,x} + ib_{i,y}$, and where $\eta_{\mathbf{b}} = +1$ for $\mathbf{b}/2 \in \text{RLV}$ and -1 otherwise. This allows us to extract all the dependence on the RLV

into a generalized momentum-space interaction $\tilde{V}_{\mathbf{q},s,t}$. We can then write the full Hamiltonian \hat{H}_s on the torus as a perturbation to the Hamiltonian in the LLL as follows:

$$\hat{H}_s = \sum_{\mathbf{q}} \sum_{s,t \in BZ} \tilde{V}_{\mathbf{q},s,t} f_0^{s,s-\mathbf{q}} f_0^{t,t+\mathbf{q}} c_s^\dagger c_t^\dagger c_{t+\mathbf{q}} c_s - q, \quad (14)$$

where in $\tilde{V}_{\mathbf{q},s,t} = V(\mathbf{q})(1 + \varepsilon_{\mathbf{q},s,t})$, \mathbf{q} is the momentum transfer (Here we take $w_0 = 1$ without loss of generality). The broken continuous translational symmetry from the lattice system is encoded in the perturbation:

$$\begin{aligned} \varepsilon_{\mathbf{q},s,t} = & \sum_{b_i \neq 0} w_{b_i} (\mathcal{F}_{b_i, -\mathbf{q}, s} + \mathcal{F}_{b_i, \mathbf{q}, t}) \\ & + \sum_{b_i, b_j \neq 0} w_{b_i} w_{b_j} \mathcal{F}_{b_i, -\mathbf{q}, s} \mathcal{F}_{b_j, \mathbf{q}, t}, \end{aligned} \quad (15)$$

where $\mathcal{F}_{\mathbf{b}, \mathbf{q}, t} \equiv \eta_{\mathbf{b}} e^{-\frac{1}{4}|\mathbf{b}|^2} e^{-it \times \mathbf{b}} e^{\frac{1}{2} \mathbf{b}^* \cdot \mathbf{q}}$. In the case where $w_{b_i} = 0$, the Hamiltonian is equivalent to the LLL Hamiltonian in the momentum basis.

Interestingly, even beyond the linearized special case in Eq.(12), the ground state wavefunctions are invariant as exact zero energy Laughlin states with arbitrary choices of w_{b_i} for $V(\mathbf{q}) = V_1$, with the exact three-fold degeneracy at $\nu = 1/3$. This implies that the universal properties of the GM still hold, including the chirality [43, 77, 78]. This observation has been confirmed by extensive numerical computations. We conjecture the universal behavior can be analytically proven by expanding Eq. 15 in the orthonormal basis of the generalized pseudopotentials (PPs). Crucially, the perturbation for nonzero w_{b_i} is *holomorphic* in q , apart from in $V_1(\mathbf{q})$, reflecting the chiral nature of the IFB. These holomorphic terms do not compromise the Hermiticity of the Hamiltonian in the torus geometry [90]. Because of this holomorphicity, the expansion in terms of generalized pseudopotentials only involves the $V_{1,m}^+$ terms [91]:

$$V_1(\mathbf{q}) \varepsilon_{\mathbf{q},s,t} = \sum_m \lambda_{1,m,s,t} V_{1,m}^+(\mathbf{q}), \quad (16)$$

where $V_{1,m}^+(\mathbf{q}) \sim q^m \mathcal{L}_1^m(|q|^2)$ is the generalized PP with $\mathcal{L}_n^m(x)$ the generalized Laguerre polynomial $\mathcal{L}_n^m(x)$ [61, 82, 92]. Physically, the $V_{1,m}^+$ pseudopotentials only energetically penalize a pair of electrons if its relative angular momentum is $\Delta L = 1$. The Laughlin model state and its quasihole states thus have exact zero energy no matter how complicated $\lambda_{1,m,s,t}$ are, as any pair of electrons has at least $\Delta L \geq 3$.

One can thus understand the vanishing lifetime of the GM from \hat{H}_s with nonzero w_{b_i} in a rather transparent manner: the many-body GM, from the geometric deformation of the ground state, is invariant with w_{b_i} . In the thermodynamic limit, the ground state (and the zero energy quasihole states) exhibits an emergent guiding center rotational symmetry, as it is *identical* to the Laughlin state in the LLL apart from the single particle normalization. This emergent symmetry arises even

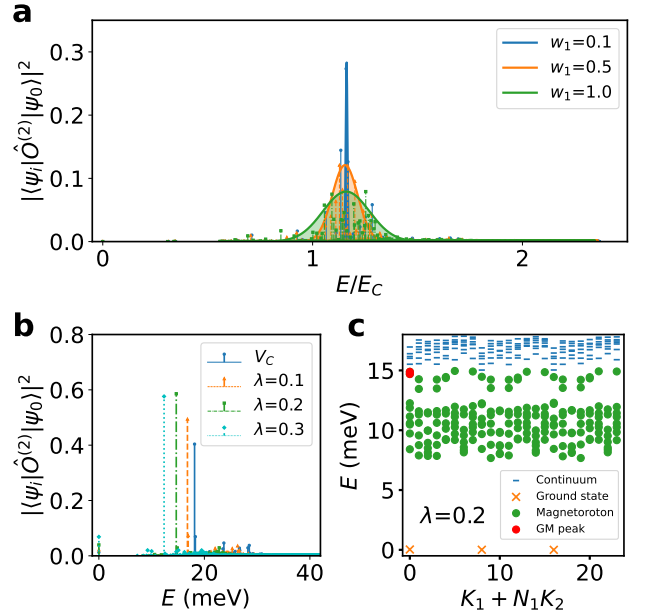


FIG. 4. **(a) Spectral function of \hat{H}_s with different perturbation strengths.** A Gaussian fit is applied to track the evolution of the GM peak, which diminishes rapidly with increasing perturbation strength. The w_1 in the legend is relative to the cTBG value. The spectral peaks decrease monotonically with larger w_1 . **(b) Spectral functions with modified Coulomb interaction V_{ZDS} in $t\text{MoTe}_2$.** The system size is with 24 orbitals at the hole filling $\nu = -2/3$. Incorporating the finite-thickness effect described by V_{ZDS} shifts the GM peak further away from the continuum. This separation isolates the GM from other excitations and enhances its lifetime, as shown by the higher peaks. **(c) Spectrum of V_{ZDS} at $\lambda = 0.2$.** The red dot shows the position of the GM peak presented in **b**, gapped from the continuum. Here (K_1, K_2) gives the position in the first Brillouin zone with $N_1 = 4$ as the number of sites along one of the primitive lattice vectors.

though the interaction explicitly breaks the continuous rotational symmetry in the moiré IFBs. On the contrary, the gapped excitations in the continuum are strongly affected by Eq.(16) and become highly anisotropic, mixing different angular momentum sectors. Naturally the rotationally invariant GM in such systems will be strongly scattered if it lies within the continuum, in contrast to the cases in the LLs.

The emergent rotational symmetry should also be robust in realistic systems or more general models (e.g., beyond the model interaction or the chiral limit), as long as the topological phase itself is robust with a large incompressible gap compared to the perturbations to the chiral interaction. This is because the perturbations to the chiral interaction are suppressed by the incompressibility gap, rendering the ground state (and thus the GM) only slightly anisotropic. In contrast, $\varepsilon_{\mathbf{q},s,t}$ significantly perturbs the continuous gapped excitations of

\hat{H}_{LLL} , scattering the excitations between different angular momentum sectors. In particular, the spin-2 modes present in the LLL spectrum, responsible for the narrow spectral peak, will scatter with other higher spin modes by $\varepsilon_{\mathbf{q},s,t}$. This explanation is numerically confirmed by Fig. 4a, where the GM peak of \hat{H}_s rapidly decreases with increasing w_1 .

Thus for moiré systems realizing Chern bands that well approximate the IFB conditions (e.g., the TBG and MoTe₂ systems), the main physics is captured by the dynamical properties of \hat{H}_s . There is an explicit breaking of rotational symmetry of the interaction within the flat band, for any interaction supporting a robust topological phase (e.g., Coulomb or V_1 interaction). Such interactions can always be expressed as an anisotropic perturbation to \hat{H}_{LLL} , just like Eq. 14 (but with different $\varepsilon_{\mathbf{q},s,t}$ depending on the details of the system). Interestingly, as explained above, the ground state (and thus the GM emerging from the geometric deformation of the ground state) is hardly perturbed by $\varepsilon_{\mathbf{q},s,t}$ due to the presence of the incompressibility gap, as argued above for \hat{H}_s and also numerically verified for other models. The scattering of the GM by the anisotropic continuum is the fundamental reason why GMs fail to exhibit a long lifetime in moiré systems.

It is useful to recall that microscopic Hamiltonians of the moiré systems (or lattice systems in general) only have discrete rotational symmetry (e.g. C_3 symmetry in TBG), one thus naively would expect the quantum fluid to have only discrete rotational symmetry both below or above the incompressibility gap. Geometric excitations from the ground state thus seem complicated, and not much can be said about their dynamics other than from numerical computations with finite system sizes. The results from numerical computations are challenging to interpret due to the small DOS, as discussed in the previous section. Generically one would argue that the GMs (which may not even be well defined due to discrete symmetry) are naturally weak and so the spectral peaks found in numerics are surprising. The discovery that the ground state (or any states below the gap) and thus the geometric excitation have emergent continuous rotational symmetry, while gapped excitations do not, leads to two main messages: firstly it gives a firm understanding on why GMs in the continuum will have vanishing lifetime despite the numerical results from small systems; secondly the GMs are still well defined and they can in principle be measured when properly tuned, as we will discuss in detail in the next section.

VI. EXPERIMENTAL DISCUSSIONS BASED ON *t*TMD SYSTEMS

We have demonstrated that GMs in moiré systems (or periodic lattice systems in general) are intrinsically weak due to the robustness of the isotropic ground state of the topological phases, even if the Hamiltonian explic-

itly breaks continuous rotational symmetry. As a result, measuring GMs experimentally becomes extremely challenging when the GM energy lies within the continuum. Additionally, caution is required when interpreting numerical results for finite-size systems with Coulomb interactions (e.g., in Ref.[87]). Thus to detect GMs in experimental systems, it is crucial to tune the GM energy below the continuum. This ensures that, like the ground state, they are protected by an energy gap to the continuum and exhibit an emergent guiding center rotational symmetry. The key principle for tuning the interaction is to reduce its short-range components [86, 93, 94]. Under these conditions, the DOS at the GM energy no longer diverges with system size, and a numerically observed narrow spectral peak for small system sizes can remain robust in the thermodynamic limit.

The analytical results from previous sections are also applicable to various more realistic models beyond the IFB limit, as we have checked extensively with numerics. Here it is useful to focus on one realistic model and calculate the GM spectral functions for *t*MoTe₂, where FCI phases have been observed in the absence of magnetic fields [47–50]. In Fig. 4, we present results for a continuum model of *t*MoTe₂ with the parameters $(V, \psi, w, \epsilon) = (20.8\text{meV}, 107.7^\circ, -23.8\text{meV}, 5)$ at the twist angle 3.89° and the hole filling $\nu = -2/3$ (so the chirality is opposite to the IFB results above) [95, 96]. The chiral graviton operators are taken as the $L = 2$ representation of the D_3 group to fulfill the periodic boundary conditions and moiré lattice symmetry. The GM spectral function shows that *t*MoTe₂ exhibits the same behavior as IFBs. Specifically, under pure Coulomb interaction, the GM peak is located near the continuum boundary, with a magnitude of approximately 0.4. However, with the V_1 pseudopotential, the peak shifts deeper into the continuum, reducing in magnitude to around 0.03. These results are in excellent agreement with those observed for IFBs.

In existing experimental setups, a dual-gate geometry is commonly used to induce hole doping, which introduces a screening effect on the Coulomb interaction. Accordingly, most theoretical calculations consider Coulomb interactions screened by symmetric dual gates [96–98], consistent with experimental configurations [47–50]:

$$V_{SC}(\mathbf{q}) = \frac{2\pi e^2 \tanh(\xi|\mathbf{q}|/2)}{\epsilon |\mathbf{q}|}, \quad (17)$$

where ξ represents the screening length, corresponding to the distance to the gate plates. The screening effect suppresses the long-range components, effectively enhancing the short-range components. This would increase the GM energy relative to the continuum. However, its impact is limited since ξ is typically several times larger than the moiré lattice constant a_M in common experimental setups [48, 49]. This means that we expect the GM to have similar strength for the realistic screened interaction as it does for the Coulomb interaction that we considered previously.

To strengthen the GM, we propose a potential interaction mechanism to effectively soften the GM:

$$V_{ZDS}(\mathbf{q}) = \frac{2\pi e^2}{\epsilon} \cdot \frac{e^{-\lambda \cdot a_M \cdot |\mathbf{q}|}}{|\mathbf{q}|} \quad (18)$$

Such interaction is the Zhang-Das-Sarma (ZDS) potential, commonly used to describe finite-thickness effects in QH systems [99, 100]. This interaction has smaller short-range components than the standard Coulomb interaction, making it effective in reducing the GM energy. Here, $\lambda \cdot a_M$ represents the “thickness” of the wavefunctions in $t\text{MoTe}_2$, accounting for the spread of electronic wavefunctions in the out-of-plane direction. As shown in Fig. 4c, a slight increase in λ shifts the GM peak downward from the continuum boundary and enhances its magnitude compared to the pure Coulomb interaction as confirmed by Fig. 4b. Experimentally, this increase in the effective thickness of the $t\text{MoTe}_2$ sample can be achieved by inserting a thin dielectric medium between the twisted layers or using twisted multilayer MoTe_2 . However, it is crucial to maintain the interlayer distance within an op-

timal range, as an excessive increase in λ may induce phase transitions that destabilize the FCI phase, which requires further investigation and will be left for future studies.

ACKNOWLEDGMENTS

We thank Z. Y. Meng, X. Shen, Z. Liu, L. Du, M. Long, H. Lu, Q. Xu, B. Peng, and Ha Q. Trung for useful discussions. This work is supported by the NTU grant for the National Research Foundation, Singapore under the NRF fellowship award (NRF-NRFF12-2020-005), and Singapore Ministry of Education (MOE) Academic Research Fund Tier 3 Grant (No. MOE-MOET32023-0003) “Quantum Geometric Advantage”. J. H. and Y. B. K. are supported by the Natural Sciences and Engineering Research Council (NSERC) of Canada and the Center for Quantum Materials at the University of Toronto. D.X.N. is supported by the Institute for Basic Science in Korea through the Project IBS-R024-D1.

-
- [1] J. P. Eisenstein, L. N. Pfeiffer, and K. W. West, Precursors to exciton condensation in quantum Hall bilayers, *Phys. Rev. Lett.* **123**, 066802 (2019).
- [2] Y. Xu, S. Liu, D. A. Rhodes, K. Watanabe, T. Taniguchi, J. Hone, V. Elser, K. F. Mak, and J. Shan, Correlated insulating states at fractional fillings of moiré superlattices, *Nature* **587**, 214 (2020).
- [3] N. J. Zhang, R. Q. Nguyen, N. Batra, X. Liu, K. Watanabe, T. Taniguchi, D. E. Feldman, and J. I. A. Li, Excitons in the fractional quantum Hall effect, *Nature* **637**, 327 (2025).
- [4] S. Wu, L. M. Schoop, I. Sodemann, R. Moessner, R. J. Cava, and N. P. Ong, Charge-neutral electronic excitations in quantum insulators, *Nature* **635**, 301 (2024).
- [5] G. Wagner and D. X. Nguyen, Successive electron-vortex binding in quantum Hall bilayers at $\nu = \frac{1}{4} + \frac{3}{4}$, *Phys. Rev. B* **110**, 195106 (2024).
- [6] P. Kumar and F. Haldane, Neutral excitations of quantum Hall states: A density matrix renormalization group study, *Physical Review B* **106**, 075116 (2022).
- [7] U. Khanna, M. Goldstein, and Y. Gefen, Emergence of neutral modes in Laughlin-like fractional quantum Hall phases, *Phys. Rev. Lett.* **129**, 146801 (2022).
- [8] A. C. Balram, G. Sreejith, and J. Jain, Splitting of the Girvin-Macdonald-Platzman density wave and the nature of chiral gravitons in the fractional quantum Hall effect, *Phys. Rev. Lett.* **133**, 246605 (2024).
- [9] Y. Liu, T. Zhao, and T. Xiang, Resolving geometric excitations of fractional quantum Hall states, *Physical Review B* **110**, 195137 (2024).
- [10] H. Lu, B.-B. Chen, H.-Q. Wu, K. Sun, and Z. Y. Meng, Thermodynamic response and neutral excitations in integer and fractional quantum anomalous Hall states emerging from correlated flat bands, *Phys. Rev. Lett.* **132**, 236502 (2024).
- [11] J. Liang, Z. Liu, Z. Yang, Y. Huang, U. Wurstbauer, C. R. Dean, K. W. West, L. N. Pfeiffer, L. Du, and A. Pinczuk, Evidence for chiral graviton modes in fractional quantum Hall liquids, *Nature* **628**, 78 (2024).
- [12] M. Long, H. Lu, H.-Q. Wu, and Z. Y. Meng, Spectra of magnetoroton and chiral graviton modes of fractional Chern insulator (2025), arXiv:2501.00247 [cond-mat.str-el].
- [13] X.-G. Wen and Q. Niu, Ground-state degeneracy of the fractional quantum Hall states in the presence of a random potential and on high-genus Riemann surfaces, *Physical Review B* **41**, 9377 (1990).
- [14] X.-G. Wen, Topological orders and edge excitations in fractional quantum Hall states, *Advances in Physics* **44**, 405 (1995).
- [15] F. D. M. Haldane, Geometrical description of the fractional quantum Hall effect, *Phys. Rev. Lett.* **107**, 116801 (2011).
- [16] B. Yang, Z.-X. Hu, Z. Papić, and F. D. M. Haldane, Model wave functions for the collective modes and the magnetoroton theory of the fractional quantum Hall effect, *Phys. Rev. Lett.* **108**, 256807 (2012).
- [17] B. Yang, Z. Papić, E. Rezayi, R. Bhatt, and F. Haldane, Band mass anisotropy and the intrinsic metric of fractional quantum Hall systems, *Physical Review B—Condensed Matter and Materials Physics* **85**, 165318 (2012).
- [18] Y. Ren, Z. Qiao, and Q. Niu, Topological phases in two-dimensional materials: a review, *Reports on Progress in Physics* **79**, 066501 (2016).
- [19] K. v. Klitzing, G. Dorda, and M. Pepper, New method for high-accuracy determination of the fine-structure constant based on quantized Hall resistance, *Phys. Rev. Lett.* **45**, 494 (1980).
- [20] D. C. Tsui, H. L. Stormer, and A. C. Gossard, Two-dimensional magnetotransport in the extreme quantum limit, *Phys. Rev. Lett.* **48**, 1559 (1982).

- [21] S. Wu, Z. Zhang, K. Watanabe, T. Taniguchi, and E. Y. Andrei, Chern insulators, van Hove singularities and topological flat bands in magic-angle twisted bilayer graphene, *Nature Materials* **20**, 488 (2021).
- [22] Y. Xie, A. T. Pierce, J. M. Park, D. E. Parker, E. Khalaf, P. Ledwith, Y. Cao, S. H. Lee, S. Chen, P. R. Forrester, K. Watanabe, T. Taniguchi, A. Vishwanath, P. Jarillo-Herrero, and A. Yacoby, Fractional Chern insulators in magic-angle twisted bilayer graphene, *Nature* **600**, 439 (2021).
- [23] D. Sheng, Z.-C. Gu, K. Sun, and L. Sheng, Fractional quantum Hall effect in the absence of Landau levels, *Nat. Commun.* **2**, <https://doi.org/10.1038/ncomms1380> (2011).
- [24] N. Regnault and B. A. Bernevig, Fractional Chern insulator, *Phys. Rev. X* **1**, 021014 (2011).
- [25] S. A. Parameswaran, R. Roy, and S. L. Sondhi, Fractional quantum Hall physics in topological flat bands, *Comptes Rendus Physique* **14**, 816 (2013).
- [26] E. M. Spanton, A. A. Zibrov, H. Zhou, T. Taniguchi, K. Watanabe, M. P. Zaletel, and A. F. Young, Observation of fractional Chern insulators in a van der Waals heterostructure, *Science* **360**, 62 (2018).
- [27] X. Huang, T. Wang, S. Miao, C. Wang, Z. Li, Z. Lian, T. Taniguchi, K. Watanabe, S. Okamoto, D. Xiao, S.-F. Shi, and Y.-T. Cui, Correlated insulating states at fractional fillings of the WS₂/WSe₂ moiré lattice, *Nature Physics* **17**, 715 (2021).
- [28] W. Zhao, K. Kang, Y. Zhang, P. Knüppel, Z. Tao, L. Li, C. L. Tschirhart, E. Redekop, K. Watanabe, T. Taniguchi, A. F. Young, J. Shan, and K. F. Mak, Realization of the Haldane Chern insulator in a moiré lattice, *Nature Physics* **20**, 275 (2024).
- [29] S. M. Girvin, A. H. MacDonald, and P. M. Platzman, Magneto-roton theory of collective excitations in the fractional quantum Hall effect, *Phys. Rev. B* **33**, 2481 (1986).
- [30] A. Pinczuk, B. S. Dennis, L. N. Pfeiffer, and K. West, Observation of collective excitations in the fractional quantum Hall effect, *Phys. Rev. Lett.* **70**, 3983 (1993).
- [31] A. Pinczuk, B. Dennis, L. Pfeiffer, and K. West, Light scattering by collective excitations in the fractional quantum hall regime, *Physica B: Condensed Matter* **249-251**, 40 (1998).
- [32] D.-H. Lee and S.-C. Zhang, Collective excitations in the Ginzburg-Landau theory of the fractional quantum Hall effect, *Phys. Rev. Lett.* **66**, 1220 (1991).
- [33] P. M. Platzman and S. He, Resonant Raman scattering from magneto rotons in the fractional quantum Hall liquid, *Physica Scripta* **1996**, 167 (1996).
- [34] I. I. Kogan, Area-preserving diffeomorphism, W_∞ and $\mathcal{U}_q[sl(2)]$ in Chern-Simons theory and the quantum Hall system, *International Journal of Modern Physics A* **09**, 3887 (1994).
- [35] S. Iso, D. Karabali, and B. Sakita, Fermions in the lowest Landau level. bosonization, W_∞ algebra, droplets, chiral bosons, *Physics Letters B* **296**, 143 (1992).
- [36] A. Cappelli, C. A. Trugenberger, and G. R. Zemba, Infinite symmetry in the quantum Hall effect, *Nuclear Physics B* **396**, 465 (1993).
- [37] M. Flohr and R. Varnhagen, Infinite symmetry in the fractional quantum Hall effect, *Journal of Physics A: Mathematical and General* **27**, 3999 (1994).
- [38] B. Yang, Quantum geometric fluctuations in fractional quantum Hall fluids, arXiv preprint arXiv:2411.05076 (2024).
- [39] S. Golkar, D. X. Nguyen, and D. T. Son, Spectral sum rules and magneto-roton as emergent graviton in fractional quantum Hall effect, *J. High Energy Phys.* **2016** (1).
- [40] A. Gromov and D. T. Son, Bimetric theory of fractional quantum Hall states, *Phys. Rev. X* **7**, 041032 (2017).
- [41] D. X. Nguyen, K. Prabhu, A. C. Balram, and A. Gromov, Supergravity model of the Haldane-Rezayi fractional quantum Hall state, *Phys. Rev. B* **107**, 125119 (2023).
- [42] D. X. Nguyen, D. T. Son, and C. Wu, Lowest Landau level stress tensor and structure factor of trial quantum Hall wave functions (2014), arXiv:1411.3316 [cond-mat.str-el].
- [43] Y. Wang and B. Yang, Geometric fluctuation of conformal Hilbert spaces and multiple graviton modes in fractional quantum Hall effect, *Nat. Commun.* **14**, <https://doi.org/10.1038/s41467-023-38036-0> (2023).
- [44] D. X. Nguyen, F. Haldane, E. Rezayi, D. T. Son, and K. Yang, Multiple magnetorotons and spectral sum rules in fractional quantum Hall systems, *Phys. Rev. Lett.* **128**, 246402 (2022).
- [45] D. X. Nguyen and D. T. Son, Dirac composite fermion theory of general Jain sequences, *Phys. Rev. Research* **3**, 033217 (2021).
- [46] A. C. Balram, Z. Liu, A. Gromov, and Z. Papić, Very-high-energy collective states of partons in fractional quantum Hall liquids, *Phys. Rev. X* **12**, 021008 (2022).
- [47] H. Park, J. Cai, E. Anderson, Y. Zhang, J. Zhu, X. Liu, C. Wang, W. Holtzmann, C. Hu, Z. Liu, T. Taniguchi, K. Watanabe, J.-H. Chu, T. Cao, L. Fu, W. Yao, C.-Z. Chang, D. Cobden, D. Xiao, and X. Xu, Observation of fractionally quantized anomalous Hall effect, *Nature* **622**, 74 (2023).
- [48] F. Xu, Z. Sun, T. Jia, C. Liu, C. Xu, C. Li, Y. Gu, K. Watanabe, T. Taniguchi, B. Tong, J. Jia, Z. Shi, S. Jiang, Y. Zhang, X. Liu, and T. Li, Observation of integer and fractional quantum anomalous Hall effects in twisted bilayer MoTe₂, *Phys. Rev. X* **13**, 031037 (2023).
- [49] J. Cai, E. Anderson, C. Wang, X. Zhang, X. Liu, W. Holtzmann, Y. Zhang, F. Fan, T. Taniguchi, K. Watanabe, Y. Ran, T. Cao, L. Fu, D. Xiao, W. Yao, and X. Xu, Signatures of fractional quantum anomalous Hall states in twisted MoTe₂, *Nature* **622**, 63 (2023).
- [50] Y. Zeng, Z. Xia, K. Kang, J. Zhu, P. Knüppel, C. Vaswani, K. Watanabe, T. Taniguchi, K. F. Mak, and J. Shan, Thermodynamic evidence of fractional Chern insulator in moiré MoTe₂, *Nature* **622**, 69 (2023).
- [51] E. Redekop, C. Zhang, H. Park, J. Cai, E. Anderson, O. Sheekey, T. Arp, G. Babikyan, S. Salters, K. Watanabe, T. Taniguchi, M. E. Huber, X. Xu, and A. F. Young, Direct magnetic imaging of fractional Chern insulators in twisted MoTe₂, *Nature* **635**, 584 (2024).
- [52] Z. Ji, H. Park, M. E. Barber, C. Hu, K. Watanabe, T. Taniguchi, J.-H. Chu, X. Xu, and Z.-X. Shen, Local probe of bulk and edge states in a fractional Chern insulator, *Nature* **635**, 578 (2024).
- [53] E. Tang, J.-W. Mei, and X.-G. Wen, High-temperature fractional quantum Hall states, *Phys. Rev. Lett.* **106**, 236802 (2011).
- [54] K. Sun, Z. Gu, H. Katsura, and S. Das Sarma, Nearly flatbands with nontrivial topology, *Phys. Rev. Lett.*

- 106**, 236803 (2011).
- [55] T. Neupert, L. Santos, C. Chamon, and C. Mudry, Fractional quantum Hall states at zero magnetic field, *Phys. Rev. Lett.* **106**, 236804 (2011).
- [56] Y.-F. Wang, Z.-C. Gu, C.-D. Gong, and D. Sheng, Fractional quantum Hall effect of hard-core bosons in topological flat bands, *Phys. Rev. Lett.* **107**, 146803 (2011).
- [57] Z. Liu and E. J. Bergholtz, Recent developments in fractional Chern insulators, in *Encyclopedia of Condensed Matter Physics (Second Edition)*, edited by T. Chakraborty (Academic Press, Oxford, 2024) second edition ed., pp. 515–538.
- [58] R. Roy, Band geometry of fractional topological insulators, *Phys. Rev. B* **90**, 165139 (2014).
- [59] M. Claassen, C. H. Lee, R. Thomale, X.-L. Qi, and T. P. Devereaux, Position-momentum duality and fractional quantum Hall effect in Chern insulators, *Phys. Rev. Lett.* **114**, 236802 (2015).
- [60] B. Mera and T. Ozawa, Kähler geometry and Chern insulators: Relations between topology and the quantum metric, *Phys. Rev. B* **104**, 045104 (2021).
- [61] J. Wang, J. Cano, A. J. Millis, Z. Liu, and B. Yang, Exact Landau level description of geometry and interaction in a flatband, *Phys. Rev. Lett.* **127**, 246403 (2021).
- [62] B. Estienne, N. Regnault, and V. Crépel, Ideal Chern bands as Landau levels in curved space, *Phys. Rev. Res.* **5**, L032048 (2023).
- [63] P. J. Ledwith, A. Vishwanath, and D. E. Parker, Vortexability: A unifying criterion for ideal fractional Chern insulators, *Phys. Rev. B* **108**, 205144 (2023).
- [64] S. A. Parameswaran, R. Roy, and S. L. Sondhi, Fractional Chern insulators and the W_∞ algebra, *Phys. Rev. B* **85**, 241308 (2012).
- [65] G. Murthy and R. Shankar, Hamiltonian theory of fractionally filled Chern bands, *Phys. Rev. B* **86**, 195146 (2012).
- [66] E. Dobardžić, M. V. Milovanović, and N. Regnault, Geometrical description of fractional Chern insulators based on static structure factor calculations, *Phys. Rev. B* **88**, 115117 (2013).
- [67] X. Hu, M. Kargarian, and G. A. Fiete, Topological insulators and fractional quantum Hall effect on the ruby lattice, *Phys. Rev. B* **84**, 155116 (2011).
- [68] R. Bistritzer and A. H. MacDonald, Moiré bands in twisted double-layer graphene, *Proc. Natl. Acad. Sci.* **108**, 12233 (2011).
- [69] N. Bultinck, E. Khalaf, S. Liu, S. Chatterjee, A. Vishwanath, and M. P. Zaletel, Ground state and hidden symmetry of magic-angle graphene at even integer filling, *Phys. Rev. X* **10**, 031034 (2020).
- [70] P. J. Ledwith, G. Tarnopolsky, E. Khalaf, and A. Vishwanath, Fractional Chern insulator states in twisted bilayer graphene: An analytical approach, *Physical Review Research* **2**, 023237 (2020).
- [71] M. Koshino, N. F. Yuan, T. Koretsune, M. Ochi, K. Kuroki, and L. Fu, Maximally localized Wannier orbitals and the extended Hubbard model for twisted bilayer graphene, *Phys. Rev. X* **8**, 031087 (2018).
- [72] S. Carr, S. Fang, Z. Zhu, and E. Kaxiras, Exact continuum model for low-energy electronic states of twisted bilayer graphene, *Phys. Rev. Research* **1**, 013001 (2019).
- [73] J. Dong, J. Wang, P. J. Ledwith, A. Vishwanath, and D. E. Parker, Composite Fermi liquid at zero magnetic field in twisted MoTe_2 , *Phys. Rev. Lett.* **131**, 136502 (2023).
- [74] Y.-H. Du, U. Mehta, D. X. Nguyen, and D. T. Son, Volume-preserving diffeomorphism as nonabelian higher-rank gauge symmetry, *SciPost Phys.* **12**, 050 (2022).
- [75] K. Yang, Acoustic wave absorption as a probe of dynamical geometrical response of fractional quantum Hall liquids, *Phys. Rev. B* **93**, 161302 (2016).
- [76] Z. Liu, A. Gromov, and Z. Papić, Geometric quench and nonequilibrium dynamics of fractional quantum Hall states, *Phys. Rev. B* **98**, 155140 (2018).
- [77] S.-F. Liou, F. D. M. Haldane, K. Yang, and E. H. Rezayi, Chiral gravitons in fractional quantum Hall liquids, *Phys. Rev. Lett.* **123**, 146801 (2019).
- [78] D. X. Nguyen and D. T. Son, Probing the spin structure of the fractional quantum Hall magnetoroton with polarized Raman scattering, *Phys. Rev. Research* **3**, 023040 (2021).
- [79] The detailed discussion was given in the Supplement Material of Ref [44].
- [80] M. Kang, A. Pinczuk, B. S. Dennis, M. A. Eriksson, L. N. Pfeiffer, and K. W. West, Inelastic light scattering by gap excitations of fractional quantum Hall states at $1/3 \leq \nu \leq 2/3$, *Phys. Rev. Lett.* **84**, 546 (2000).
- [81] Z. Papić, Fractional quantum Hall effect in a tilted magnetic field, *Phys. Rev. B* **87**, 245315 (2013).
- [82] B. Yang, C. H. Lee, C. Zhang, and Z.-X. Hu, Anisotropic pseudopotential characterization of quantum Hall systems under a tilted magnetic field, *Phys. Rev. B* **96**, 195140 (2017).
- [83] F. D. M. Haldane, Fractional quantization of the Hall effect: A hierarchy of incompressible quantum fluid states, *Phys. Rev. Lett.* **51**, 605 (1983).
- [84] S. A. Trugman and S. Kivelson, Exact results for the fractional quantum Hall effect with general interactions, *Phys. Rev. B* **31**, 5280 (1985).
- [85] F. D. M. Haldane and E. H. Rezayi, Periodic Laughlin-Jastrow wave functions for the fractional quantized Hall effect, *Phys. Rev. B* **31**, 2529 (1985).
- [86] Y. Wang and B. Yang, Analytic exposition of the graviton modes in fractional quantum Hall effects and its physical implications, *Phys. Rev. B* **105**, 035144 (2022).
- [87] X. Shen, C. Wang, X. Hu, R. Guo, H. Yao, C. Wang, W. Duan, and Y. Xu, Magnetorotons in moiré fractional Chern insulators (2024), arXiv:2412.01211 [cond-mat.str-el].
- [88] Here, we use intuition from the FQH, where the typical low-energy dynamics within a single LL are largely insensitive to normalization. As a result, the low-energy properties of fractional topological fluids remain consistent across identical topological phases in different LLs, despite variations in single-particle normalization.
- [89] Detailed derivations are given in the supplementary material.
- [90] As long as the inversion symmetry in \mathbf{b}_i vectors is preserved, the Hamiltonian will remain Hermitian. Refer to the supplementary material for more details.
- [91] Detailed derivations are given in the supplementary material.
- [92] B. Yang, Z.-X. Hu, C. H. Lee, and Z. Papić, Generalized pseudopotentials for the anisotropic fractional quantum Hall effect, *Phys. Rev. Lett.* **118**, 146403 (2017).
- [93] B. Yang, Microscopic theory for nematic fractional quantum Hall effect, *Phys. Rev. Res.* **2**, 033362 (2020).

- [94] A. C. Balram, G. J. Sreejith, and J. K. Jain, Splitting of the Girvin-MacDonald-Platzman density wave and the nature of chiral gravitons in the fractional quantum Hall effect, *Phys. Rev. Lett.* **133**, 246605 (2024).
- [95] F. Wu, T. Lovorn, E. Tutuc, I. Martin, and A. H. MacDonald, Topological insulators in twisted transition metal dichalcogenide homobilayers, *Phys. Rev. Lett.* **122**, 086402 (2019).
- [96] C. Wang, X.-W. Zhang, X. Liu, Y. He, X. Xu, Y. Ran, T. Cao, and D. Xiao, Fractional Chern insulator in twisted bilayer MoTe_2 , *Phys. Rev. Lett.* **132**, 036501 (2024).
- [97] T. Devakul, V. Crépel, Y. Zhang, and L. Fu, Magic in twisted transition metal dichalcogenide bilayers, *Nature communications* **12**, 6730 (2021).
- [98] A. P. Reddy, F. Alsallom, Y. Zhang, T. Devakul, and L. Fu, Fractional quantum anomalous Hall states in twisted bilayer MoTe_2 and WSe_2 , *Phys. Rev. B* **108**, 085117 (2023).
- [99] F.-C. Zhang and S. D. Sarma, Excitation gap in the fractional quantum Hall effect: Finite layer thickness corrections, *Physical Review B* **33**, 2903 (1986).
- [100] M. R. Peterson, T. Jolicoeur, and S. Das Sarma, Orbital Landau level dependence of the fractional quantum Hall effect in quasi-two-dimensional electron layers: Finite-thickness effects, *Phys. Rev. B* **78**, 155308 (2008).